Supporting information for: Optimizing Direct Air Capture under varying weather conditions

H.M. Schellevis, J.D. de la Combé and D.W.F. Brilman

1. Numerical model description

The mass and energy balances of the numerical model of the adsorption and desorption phase are provided in equations (1) to (6). Equation (1) is the gas phase mass balance, equation (2) is the solid phase mass balance and (3) is the overall mass balance. The energy balance in equation (4) includes convective mass transfer, conductive mass transfer, reaction heat and an external energy source that depends on the design of the adsorption column. Mass transfer to the solid phase is described with an intrinsic reaction rate and internal mass transfer limitations are accounted for via the Thiele modulus approach (equations (5) and (6))[1]. For a more detailed model description and validation can be found in earlier work[2].

$$\varepsilon_r \frac{\partial c_i}{\partial t} = \frac{\partial}{\partial z}\left(D_{ax,i}\frac{\partial c_i}{\partial z} - u_g c_i\right) - (1-\varepsilon_r)\rho_s \frac{\partial q_i}{\partial t} \tag{1}$$

$$\frac{\partial q_i}{\partial t} = R_i \eta_i \tag{2}$$

$$\varepsilon_r \frac{\partial c}{\partial t} = -\frac{\partial (u_g c)}{\partial z} - (1-\varepsilon_r)\rho_s \sum_{i=1}^{n} \frac{\partial q_i}{\partial t} \tag{3}$$

$$\left((1-\varepsilon_r)\rho_s C_{p,s} + \varepsilon_r \rho_g C_{p,g}\right)\frac{\partial T}{\partial t} = \frac{\partial}{\partial z}\left(\lambda_{s,eff}\frac{\partial T}{\partial z} - u_g \rho_g C_{p,g} T\right) + (1-\varepsilon_r)\rho_s \sum_{i=1}^{n} \Delta_r H_i \frac{\partial q_i}{\partial t} + Q_{source} \tag{4}$$

$$\eta_i = \frac{\int\int\int R_{ads,i}(c_i, q_i)\,dV}{R_{ads,i}(c_{bulk}, q_{av})} \approx \frac{3}{\phi_{th}}\frac{\phi_{th}\coth(\phi_{th}) - 1}{\phi_{th}} \tag{5}$$

$$\phi_{th} = r_p \sqrt{\frac{\rho_s k_T RT\left(1 - \left(q/q_s\right)^{t_h}\right)^{\frac{1}{t_h}}}{D_p}} \tag{6}$$

The numerical framework is showcased for a specific sorbent: Lewatit® VP OC 1065. Besides CO_2, this sorbent also adsorbs H_2O[3]. The intrinsic reaction rate of CO_2 is described with equation (7)[4] and the reaction rate for H_2O is described with equation (9)[2]. The parameters are collected in Table 1.

$$R_{CO_2} = k_T\left(RTc_{CO_2}\left(1 - \left(\frac{q_{CO_2}}{q_s}\right)^{t_h}\right)^{\frac{1}{t_h}} - \frac{q_{CO_2}}{bq_s}\right) \tag{7}$$

$$k_T = k_{0,CO_2}\exp\left(-\frac{E_{act,CO_2}}{RT}\right) \tag{8}$$

$$R_{H_2O} = k_{LDF}\frac{p_{H_2O}}{p_{H_2O}^{sat}}\left(q_{eq,H_2O} - q_{H_2O}\right) \tag{9}$$

$$k_{LDF} = k_{0,H_2O}\exp\left(-\frac{E_{act,H_2O}}{RT}\right) \tag{10}$$

The Toth isotherm is used to correlate the CO_2 equilibrium capacity as function of CO_2 partial pressure and temperature (equations (11) to (14)[2,4]. However, the CO_2 equilibrium capacity also depends on the relative humidity. An empirical correlation is used to describe the enhancement of the CO_2 equilibrium capacity as function of relative humidity following equations (15) and (16)[3].

H_2O adsorptions occurs via physisorption and is described via the GAB isotherm. It is independent of CO_2 adsorption and thus only depends on the relative humidity and temperature (equations (17) to (19))[3].

$$q_{CO_2}^{dry} = \frac{q_s b p_{CO_2}}{\left(1 + \left(b p_{CO_2}\right)^{t_h}\right)^{\frac{1}{t_h}}} \tag{11}$$

$$b = b_0\exp\left(\frac{\Delta H_0}{RT_0}\left(\frac{T_0}{T} - 1\right)\right) \tag{12}$$

$$t_h = t_{h,0} + \alpha\left(1 - \frac{T_0}{T}\right) \tag{13}$$

$$q_s = q_{s,0}\exp\left(\chi\left(1 - \frac{T}{T_0}\right)\right) f_{enh}\left(p_{H_2O}\right) \tag{14}$$

$$f_{enh}\left(p_{H_2O}\right) = \frac{q_{eq,CO_2}}{q_{CO_2}^{dry}} = 1 + a\frac{p_{H_2O}}{p_{H_2O}^{sat}} \tag{15}$$

$$a = n\exp\left(m\, q_{CO_2}^{dry}\right) \tag{16}$$

$$\frac{q_{eq,H_2O}}{q_m} = \frac{C_{GAB}k_{GAB}{}^{p_{H_2O}}/_{p_{H_2O}^{sat}}}{\left(1 - k_{GAB}{}^{p_{H_2O}}/_{p_{H_2O}^{sat}}\right)\left(1 + (C_{GAB} - 1)k_{GAB}{}^{p_{H_2O}}/_{p_{H_2O}^{sat}}\right)} \tag{17}$$

$$C_{GAB} = C_{0,GAB}\exp\left(\frac{\Delta H_C}{RT}\right) \tag{18}$$

$$k_{GAB} = k_{0,GAB}\exp\left(\frac{\Delta H_k}{RT}\right) \quad (19)$$

Table 1 – Parameters for the isotherm and reaction rate correlations of CO_2 and H_2O on Lewatit® VP OC 1065.

	Parameter	Value
CO_2 adsorption	$q_{s,0}$ (mol_{CO2} kg_s^{-1})	3.40
	χ (-)	0
	T_0 (K)	353.15
	b_0 (Pa^{-1})	93.0×10^{-5}
	ΔH_0 (kJ mol_{CO2}^{-1})	95.3
	$t_{h,0}$ (-)	0.37
	α (-)	0.33
	n (-)	2.05
	m (kg_s mol_{CO2}^{-1})	-0.85
CO_2 kinetics	k_{0,CO_2} (mol_{CO2} kg_s^{-1} Pa^{-1} s^{-1})	3.5×10^{-2}
	E_{act,CO_2} (kJ mol_{CO2}^{-1})	15.2
H_2O adsorption	q_m (mol_{H2O} kg_s^{-1})	3.10
	$C_{0,GAB}$ (-)	1.72×10^{-2}
	$k_{0,GAB}$ (-)	7.14×10^{-2}
	ΔH_C (kJ mol_{H2O}^{-1})	12.24
	ΔH_k (kJ mol_{H2O}^{-1})	5.93
H_2O kinetics	k_{0,H_2O} (s^{-1})	450
	E_{act,H_2O} (kJ mol_{H2O}^{-1})	15.2

2. Steam-assisted temperature vacuum swing process

Figure 1 shows a schematic representation of the S-TVSA process. An in-depth analysis of such process can be found in other literature[5]. We identify eight parameters that influence the performance:

1. ambient temperature,
2. ambient relative humidity,
3. gas velocity during adsorption,
4. adsorption time,
5. desorption temperature,
6. desorption pressure,
7. purge gas flowrate, and
8. desorption time.

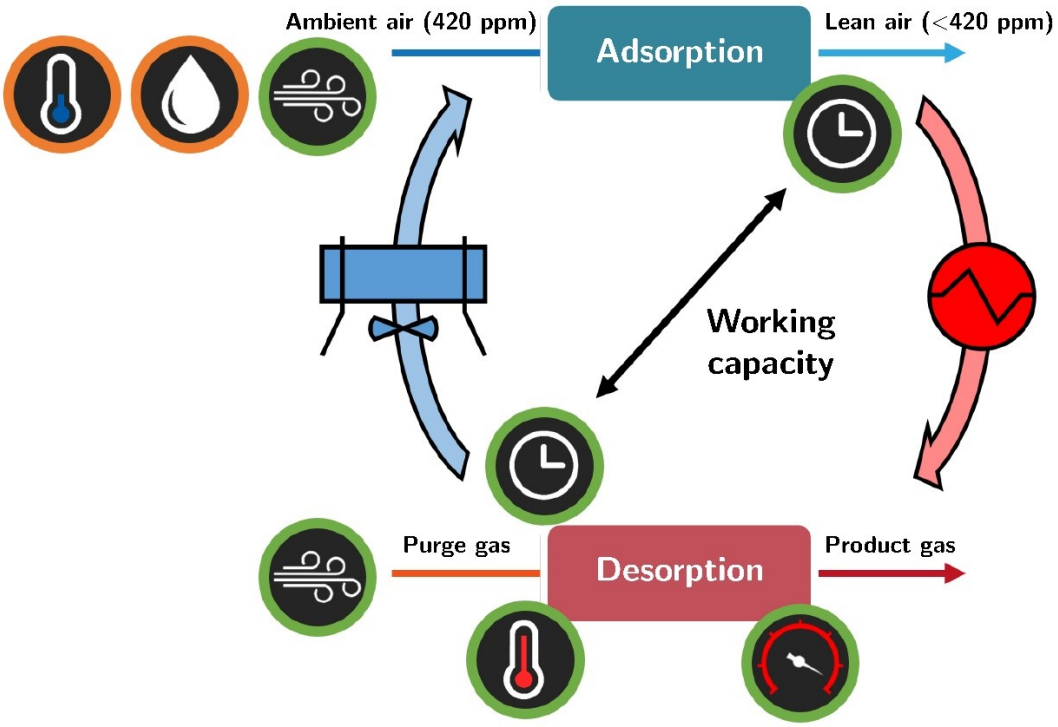

Figure 1 – Schematic of a steam-assisted temperature-vacuum swing process.

3. Walkthrough of optimization algorithm

The optimal operating parameters at minimum cost of Direct Air Capture (DAC) are obtained for certain set of ambient conditions via an optimization algorithm. This appendix provides an extensive overview including intermediate result of one of the simulations. The steps in the optimization are:

Step 1. Select a combination of ambient temperature and relative humidity.
Step 2. Perform sensitivity analysis of the adsorption phase with combinations of superficial gas velocity, lean CO_2 sorbent loading and adsorption time.
Step 3. Calculate the energy duty and productivity using guess values for the desorption parameters.
Step 4. Use the ϵ-constraint method to select potential optimal points on the Pareto front.
Step 5. Perform sensitivity analysis for the regeneration phase for combinations of desorption pressure, desorption temperature and purge gas flowrate.
Step 6. Calculate the energy duty and productivity for all combinations of operational conditions.
Step 7. Implement the chosen cost model to find the lowest cost of DAC with corresponding operational conditions.
Step 8. Repeat steps 3 to 7 using the optimal desorption parameters as guess values in step 3 until no new optimum is found.

Step 1 – Selection of ambient conditions

The ambient conditions are fixed input parameters of the optimization algorithm. This means that the minimum cost of DAC will be obtained for these certain conditions. Thus, it does not find the best

temperature and relative humidity for DAC. For that, the optimization algorithm has to be performed for all sets of ambient conditions and then find the minimum cost of DAC of those results.

The selected ambient conditions in this example are 25°C and 60% RH. This results in a CO_2 equilibrium capacity of 1.61 mol_{CO2}/kg_s and a H_2O equilibrium capacity of 3.96 mol_{H2O}/kg_s. The ambient conditions define the temperature and relative humidity of the inlet gas during adsorption and the temperature of the cooling medium during cooling. Indirectly, it also determines the initial temperature of the heating phase.

Step 2 – Sensitivity analysis of the adsorption phase for all combinations of operational parameters

The adsorption model is solved for a pre-defined set of combinations of superficial gas velocity and lean CO_2 sorbent loading. The lean H_2O sorbent loading is always set at 0 mol_{H2O}/kg_s. The ranges of these parameters are found in Table 2. The adsorption time is fixed at 20 hours, which is long enough for CO_2 to nearly reach equilibrium.

Table 2 – Range of input parameters for the adsorption sensitivity analysis.

Parameter	Minimum value	Maximum value
Superficial gas velocity ($m_g^3\ m_r^{-2}\ s^{-1}$)	0.05	0.3
Lean CO_2 sorbent loading ($mol_{CO2}\ kg_s^{-1}$)	0.01	0.3
Adsorption time (h)	0	20

The complete steam-assisted temperature vacuum swing adsorption (S-TVSA) cycle consists of an adsorption and a regeneration phase. Consequently, a steady-state is reached when the start of the adsorption phase equals the end of the regeneration phase. In principle this means that the axial concentration, sorbent loading and temperature profiles should match. However, using a uniform CO_2 loading profile resulted in nearly identical results. Therefore, a uniform profile is used, which decouples the adsorption model completely from the desorption model.

Step 3 – Calculation of key performance indicators using guess values for desorption

The energy duty and productivity are calculated for each combination and plotted according to Figure 2. These are calculated for every 10 minutes of adsorption via interpolation of the of CO_2 and H_2O sorbent loading at that adsorption time. Information from the desorption is also required, but unknown at this point. To achieve the most accurate results, the overall optimum of an evaluation with very similar ambient temperature and relative humidity is used as initial guess for the optimum desorption parameters. Another complexity is that the desorption time depends on the lean CO_2 sorbent loading. To account for this, a single desorption simulation is carried out using the guess values for desorption to obtain a relationship between lean CO_2 sorbent loading and desorption time.

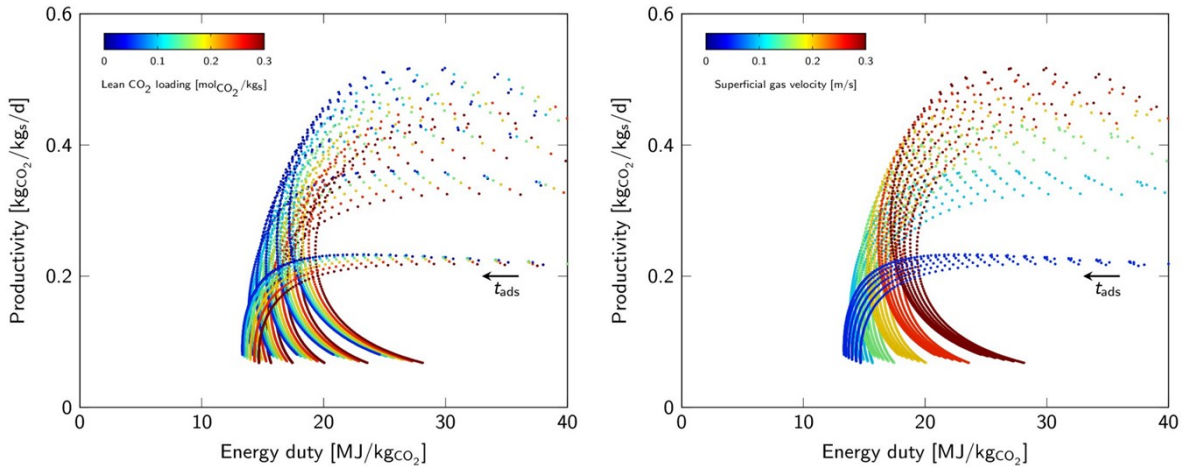

Figure 2 – Key performance indicators for the initial adsorption analysis using guess values for desorption. Both graphs contain the same data points, but the corresponding (A) lean CO_2 loading (left) and (B) superficial gas velocity (right) are shown by the colourbar.

Step 4 – Selection of Pareto points

A large set of data points are obtained and is it not feasible to perform a similar analysis for the desorption phase for each and every point. Therefore, only a small selection is made following a Pareto point analysis.

A Pareto front is formed with this type of analysis with multiple objectives. The energy duty is preferably as low as possible and the productivity is preferably as high as possible. The optimal point will then be in the top left region, which is referred to as the 'Utopia' point. It becomes clear that most combinations would never be the optimal operation point. The optimum will be one of the 'non-dominated' points, which are situated on the Pareto front. We use the ϵ-constraint method to find these Pareto points[6,7]. In this method, one objective function is optimised (productivity), while the other is constraint (energy duty) (Figure 3). First, the absolute maximum productivity and minimum energy duty are found. Then, all the points with a higher energy duty than the energy duty corresponding to the maximum productivity and all the points with a lower productivity than the productivity corresponding to the minimum energy duty are removed. These will never be an optimum. The domain between the minimum and maximum energy duty is divided into ten segments (log spacing is used to get a bit more points on the lower energy duty regime) and the point with the maximum productivity in each segment is selected for further optimization. In this manner, only a very selective set of combinations are thereby used for the regeneration analysis.

For this approach to be valid, a lower energy duty must always be beneficial. However, the energy duty consists of thermal energy and electrical energy. The costs of these energy sources depend on the actual sources of energy, but most likely are not equal. Therefore, a higher energy duty does not necessarily correspond to higher energy cost. Somehow, these different energy costs should be translated to an 'equivalent' energy duty. In this study, the thermal energy is assumed to be generated via a heat pump with a coefficient of performance (COP) of 1.7[8].

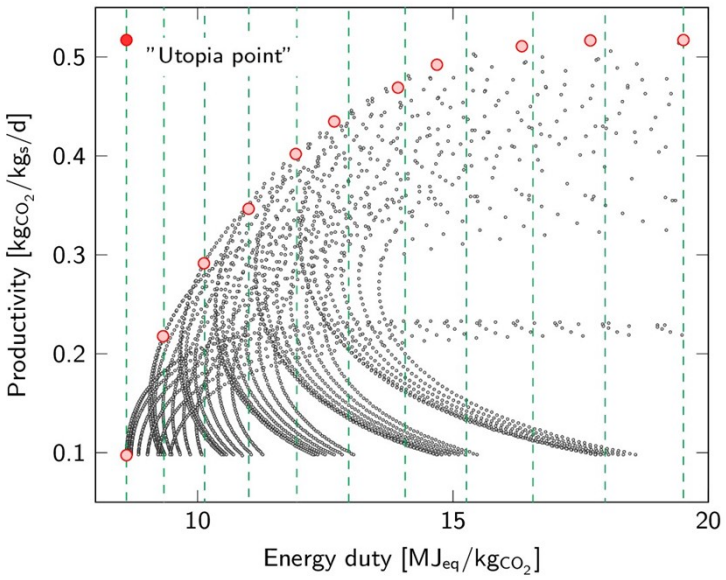

Figure 3 – Pareto front analysis using the ϵ-constraint method to find potential optimal operating points.

Step 5 – Analysis of the regeneration phase for the Pareto points

Eleven Pareto points with each a different combination of superficial gas velocity, lean CO_2 sorbent loading and adsorption time are selected via the Pareto front analysis. The regeneration phase is simulated for each of these points with varying combinations of desorption temperature, desorption pressure and purge gas flowrate. Table 3 shows the applied ranges for these values. The desorption temperature is fixed at the highest possible value. A previous studies concluded that it is beneficial for both energy duty and productivity to operate at the highest possible temperature[2].

Table 3 – Range of input parameters for the desorption sensitivity analysis.

Parameter	Minimum value	Maximum value
Desorption temperature (°C)	120	120
Desorption pressure (mbar)	15	150
Purge gas flowrate (g_{purge} kg_s^{-1} min^{-1})	0.5	6

The regeneration phase consists of consecutive heating, desorption and cooling. Heating starts at the end temperature of adsorption, in general identical to the ambient temperature. This temperature is obtained from the adsorption phase and rounded to the nearest 5°C. Each heating phase ends at 50°C. Consequently, each desorption phase starts at the same temperature, which makes the desorption phase independent from the heating phase.

Desorption only requires an initial CO_2 and H_2O sorbent loading, which are obtained from the adsorption results. Again, a uniform axial loading profile is used. The CO_2 loading is rounded to the nearest 0.05 mol_{CO2}/kg_s and the H_2O loading is rounded to the nearest 0.5 mol_{H2O}/kg_s. This saves computation time, since the desorption model does not need to be repeated for Pareto points with very similar CO_2 and H_2O loading.

Cooling requires the end temperature of desorption, which is not necessarily equal to the temperature of the heating medium (i.e. the desorption temperature). This end temperature is rounded to the nearest 5°C and heating is continued until a temperature of 40°C. That is well below the threshold of oxidative degradation. However, this is an average temperature and due to the poorly conducting

sorbent, a temperature gradient is expected. Therefore, cooling a bit further than the oxidative degradation threshold is advised to allow the complete bed temperature to be sufficiently reduced.

Step 6 – Calculation of key performance indicators

The actual productivity and energy duty are calculated from the combination of adsorption and regeneration parameters. Unlike in step 3, these do not contain guess values and are the actual key performance indicators. Figure 4 shows the new data points that are obtained from the original Pareto points. Varying the desorption pressure and purge gas flowrate improved the productivity and energy duty.

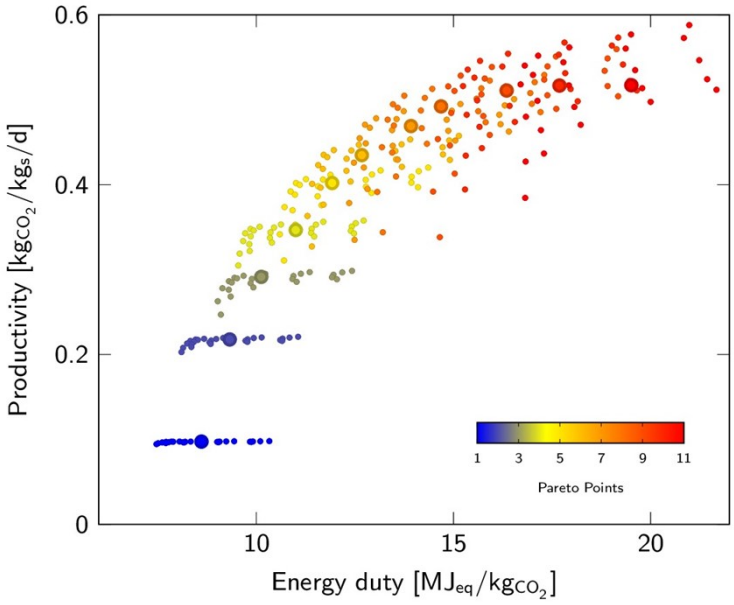

Figure 4 – Refinement of the Pareto front with the regeneration sensitivity analysis. The larger circles are the original Pareto points and the colour corresponds to the same original Pareto point.

Step 7 – implement cost model to find optimal operating point

The economic analysis is carried out using the productivity and energy duty of all points in Figure 4. The point of minimum cost of DAC will be located somewhere on the new Pareto front. Therefore, the economic analysis could be carried for these points only. However, these are straightforward calculations that require little computation time. Figure 5 shows the location of the minimum cost of DAC with the corresponding value for desorption pressure and purge gas flowrate. In additions, it visualizes the impact of both operational parameters on the energy duty and productivity.

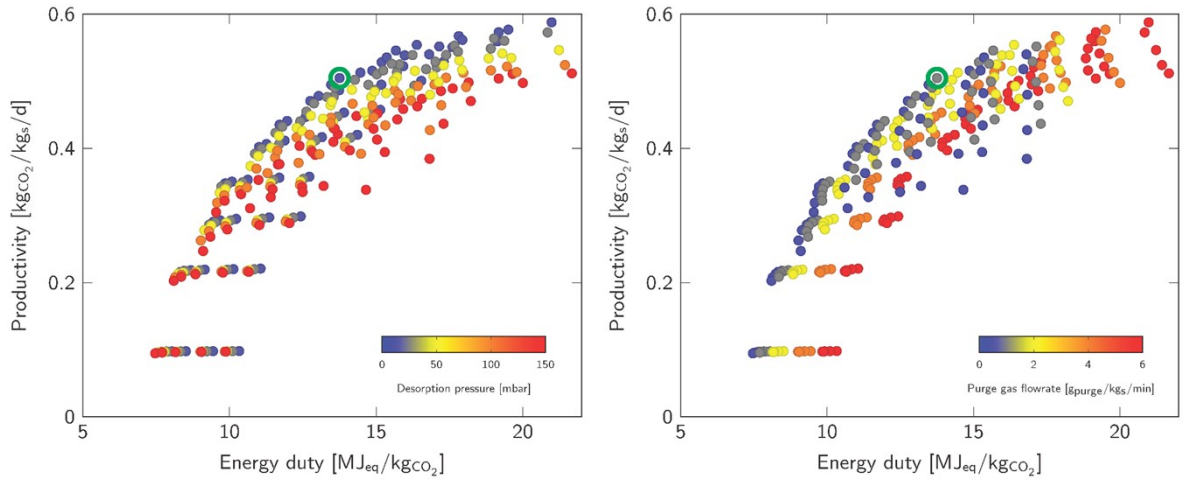

Figure 5 – Point of minimum cost of DAC with corresponding (A) desorption pressure (left) and (B) purge gas flowrate (right). Data points are equal to Figure 4.

An economic evaluation is needed to solve the trade-off between energy duty and productivity (step 7). We use a rather simple cost model proposed by Towler and Sinnott[9]. The capital costs are based on a novel (2020) 0.5 tpa DAC pilot unit[5]. The total ISBL capital investment of this pilot unit is estimated and scaled up to a capacity of 10 kton per annum. For this, we assume an economy of scale factor 0.6 following the "six-tenth rule". The operational costs include costs of sorbent, labour, maintenance, energy and additional fixed costs. Table 4 lists the assumptions used in the economic analysis. The cost of energy depends on the availability of renewable energy or waste heat. The most widely accessible form of renewable energy is solar power via either photovoltaic systems or wind power. This produces electrical energy, which is converted to thermal energy. We propose to use a high temperature heat pump and assume a COP of 1.7[8].

Table 4 – Assumptions for the economic analysis to calculate the cost of DAC.

Parameter	**Value**
CAPEX of DAC pilot unit (€$_{2020}$)	25,000
Full scale capacity (t_{CO2} yr^{-1})	10,000
Economy of scale (-)	0.6
Depreciation time (yr)	10
Sorbent lifetime (yr)	2
Sorbent costs (€ kg_s^{-1})	30
Working hours (h yr^{-1})	8,400
Salary costs (€ yr^{-1})	35,000
Maintenance costs	4% of CAPEX
Additional fixed costs	2% of CAPEX
Solar energy price (€ kWh^{-1})[10]	0.03

Step 8 - iteration with updated guess values to find overall optimum

Steps 3 to 7 are repeated using the set of optimum operational parameters obtained in step 7 as guess values in step 3. This is necessary, because the initial guess values might not have been sufficiently accurate. After the initial analysis of the energy duty and productivity, only a very small selection of points (~0.2%) were used for further analysis. It is very well possible that with more accurate guess values, other points end up at the Pareto front. Therefore, the 'optimal' results of the first optimization round are used as new guess values to check for new Pareto points. In case of a series of evaluations,

the overall optimum of an evaluation with very similar ambient conditions can be used as guess value. That will result in a rather accurate initial guess, since, for example, a 5°C difference in temperature is not expected to result in a very large difference in optimal point.

There is no need for new simulations of the adsorption phase, only the key performance indicators are calculated using updated values for the desorption parameters. A new Pareto front is obtained as shown in Figure 6, which gives a better representation of the actual key performance indicators. The same Pareto front analysis is performed to obtain eleven Pareto points.

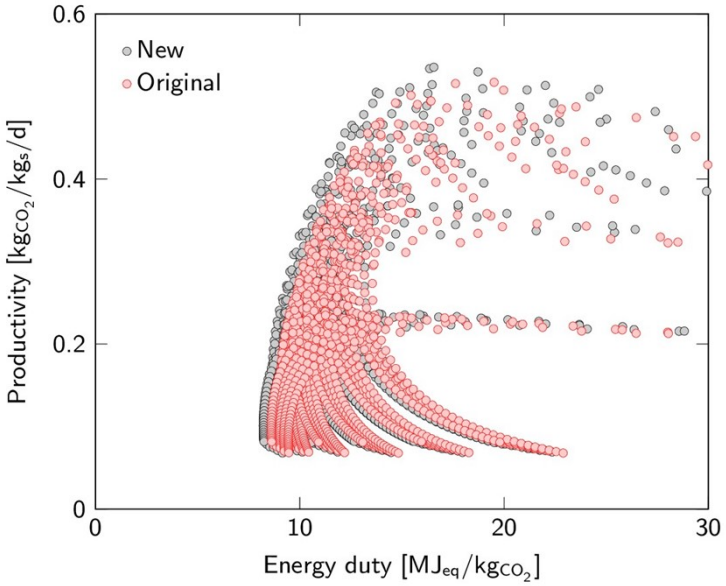

Figure 6 – Updated Pareto front using the new guess values.

The regeneration analysis is carried out using these new Pareto points. Note that these are not necessarily new combinations of superficial gas velocity, lean CO_2 sorbent loading and adsorption time. The updated desorption parameters merely caused a new value for the key performance indicators. Therefore, the regeneration analysis is only carried out for new combinations of the adsorption parameters. In the current example, five new Pareto points are found as shown in Figure 7.

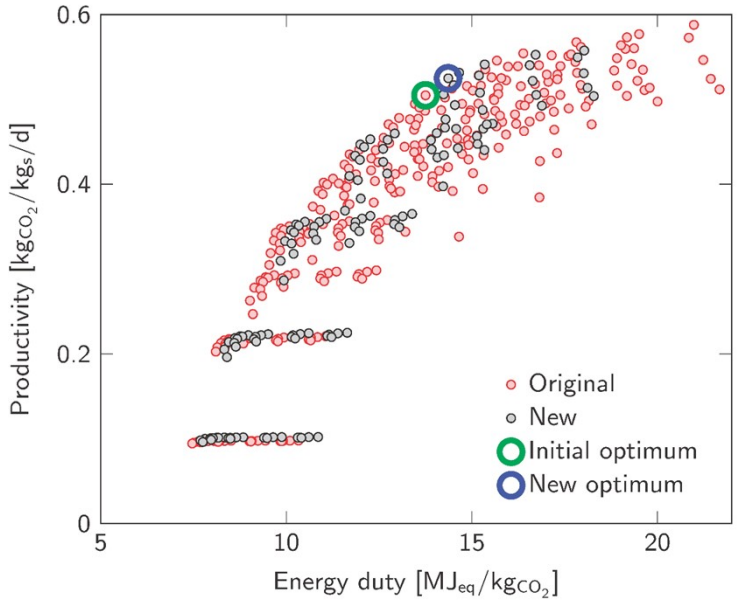

Figure 7 – Complete Pareto front after the new regeneration analysis including the original points and the new points.

As shown in Figure 7, a new optimal point is obtained, although very close to the initial optimum. Iteration can be continued until no new optimum is found. The results for an ambient temperature of 25°C and a relative humidity of 60% are summarized in Table 5. Figure 8 provides the effect of the key performance indicators on the cost of DAC. Interestingly, the minimum cost of DAC corresponds to a high value for productivity, and with that, a high value for the energy duty. In addition, the final results of the optimization of a colder, more humid ambient condition are presented (Table 5 and Figure 8). It shows a clear increase in cost of DAC for the colder conditions (310€/t_{CO2} versus 504€/t_{CO2}) and a major decrease in performance.

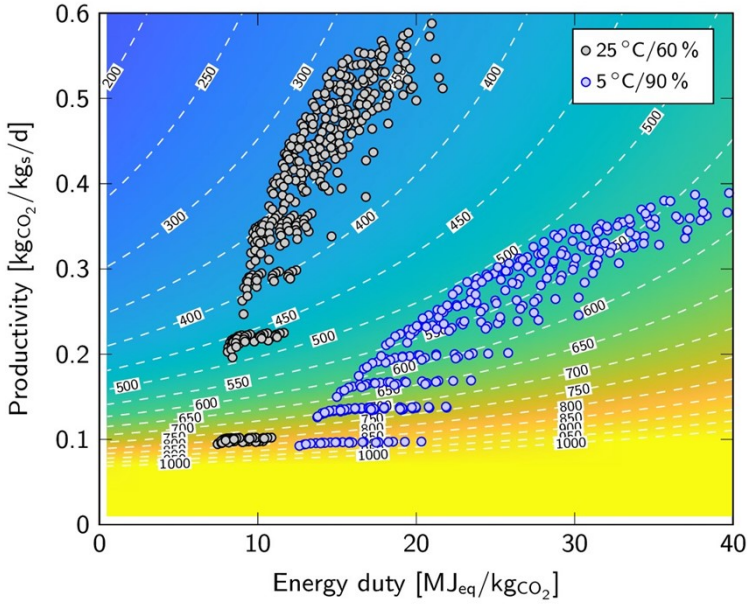

Figure 8 – Contour map of the cost of DAC as function of productivity and energy duty. The final data points from step 8 of two sets of ambient conditions are added for comparison.

Table 5 – Summary of the results of the optimization algorithm for two different ambient conditions.

Parameter	**25°C/60% RH**	**5°C/90% RH**
Cost of Direct Air Capture (€ t_{CO2}^{-1})	310	504
Energy duty (MJ kg_{CO2}^{-1})	18.8	35.0
Productivity (kg_{CO2} kgs^{-1} d^{-1})	0.50	0.28
Superficial gas velocity (m_g^3 m_r^{-2} s^{-1})	0.3	0.15
Lean CO_2 sorbent loading (mol_{CO2} kg_s^{-1})	0.05	0.01
Adsorption time (min)	90	160
Desorption temperature (°C)	120	120
Desorption pressure (mbar)	15	50
Purge gas flowrate (g_{purge} kg_s^{-1} min^{-1})	0.5	1
CO_2 working capacity (mol_{CO2} kg_s^{-1})	0.91	0.92
H_2O working capacity (mol_{H2O} kg_s^{-1})	3.9	12.3
Desorption time (min)	15	36
Heating time (min)	2	3
Cooling time (min)	9	7
Cycle time (min)	116	206
CO_2 selectivity (mol_{CO2} mol_{H2O}^{-1})	0.23	0.08
Capture efficiency (-)	0.38	0.40
Purge gas ratio (mol_{purge} mol_{CO2}^{-1})	0.46	2.2
CO_2 reaction enthalpy (MJ kg_{CO2}^{-1})	1.7	1.7
H_2O reaction enthalpy (MJ kg_{CO2}^{-1})	4.2	13.0
Sorbent sensible heat (MJ kg_{CO2}^{-1})	2.8	4.3
Reactor sensible heat (MJ kg_{CO2}^{-1})	4.5	6.8
Purge gas latent and sensible heat (MJ kg_{CO2}^{-1})	0.5	2.4
Feed compression (MJ kg_{CO2}^{-1})	1.5	0.6
Vacuum generation (MJ kg_{CO2}^{-1})	3.6	6.2
Electrical energy costs (€ t_{CO2}^{-1})	109	194
Thermal energy costs (€ t_{CO2}^{-1})	0	0
Depreciation (€ t_{CO2}^{-1})	70	98
Sorbent costs (€ t_{CO2}^{-1})	86	151
Miscellaneous costs (€ t_{CO2}^{-1})	45	62

4. Performance indicators

The energy duty and productivity are key performance indicators to determine the cost of DAC. To provide more fundamental insight in the origin of the differences between ambient conditions, Figure 9 gives the CO_2 working capacity, H_2O working capacity, cycle time, gas efficiency, pressure drop and purge gas ratio. These parameters are directly used to calculate the energy duty and productivity.

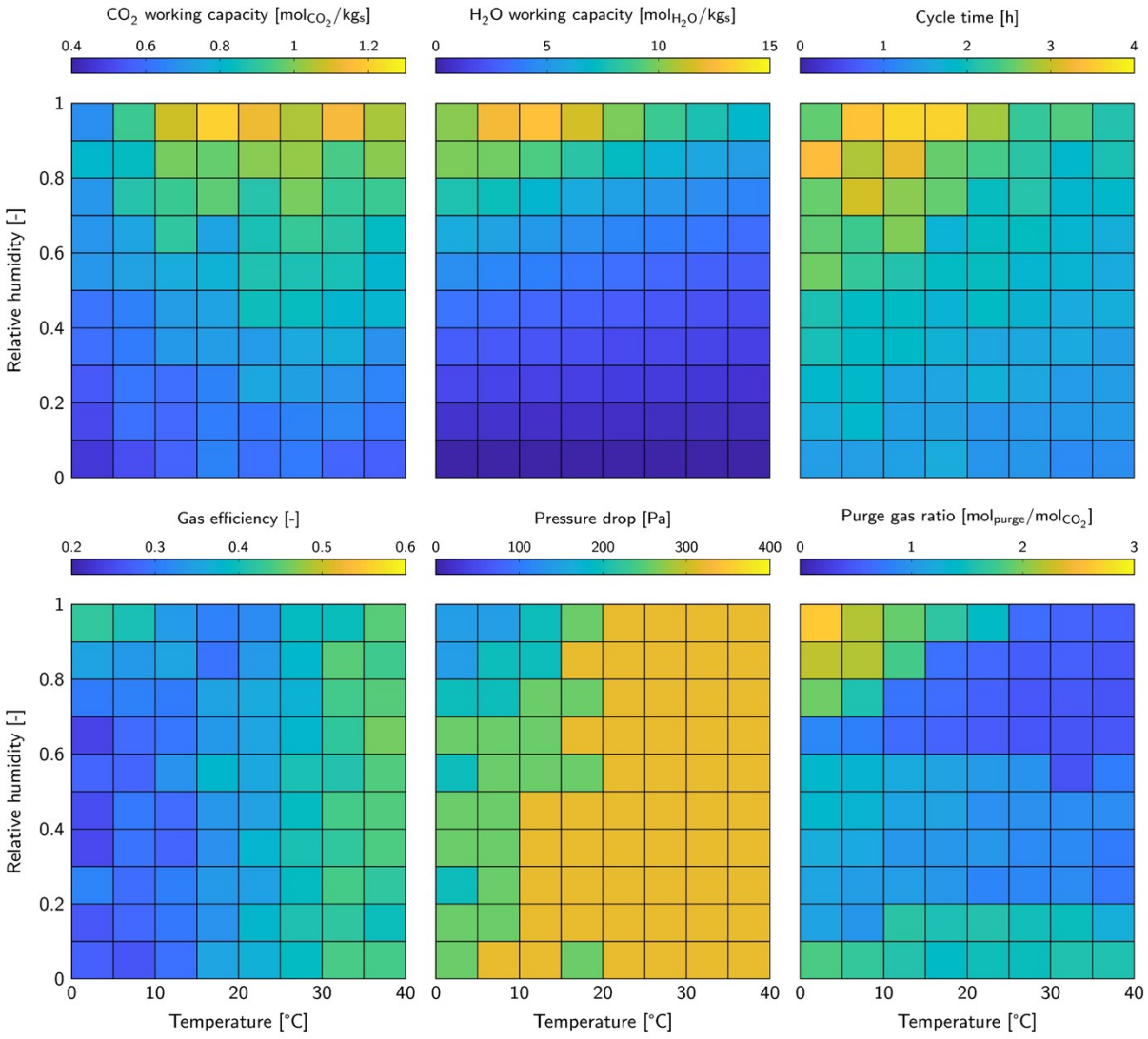

Figure 9 – Performance indicators that are used to calculate the energy duty and productivity for each combination of temperature and relative humidity.

5. Year-round climate data

The average cost of DAC for year-round operation was determined for several locations around the world. A graphical representation is provided in Figure 10 including the average cost of DAC that corresponds to the specific climate conditions. Figure 11 provides the six-hour average temperature and relative humidity for 2021 of each evaluated city. Note that the temperature ranges from -15 to 45°C, but some locations exceed this range in extreme cases.

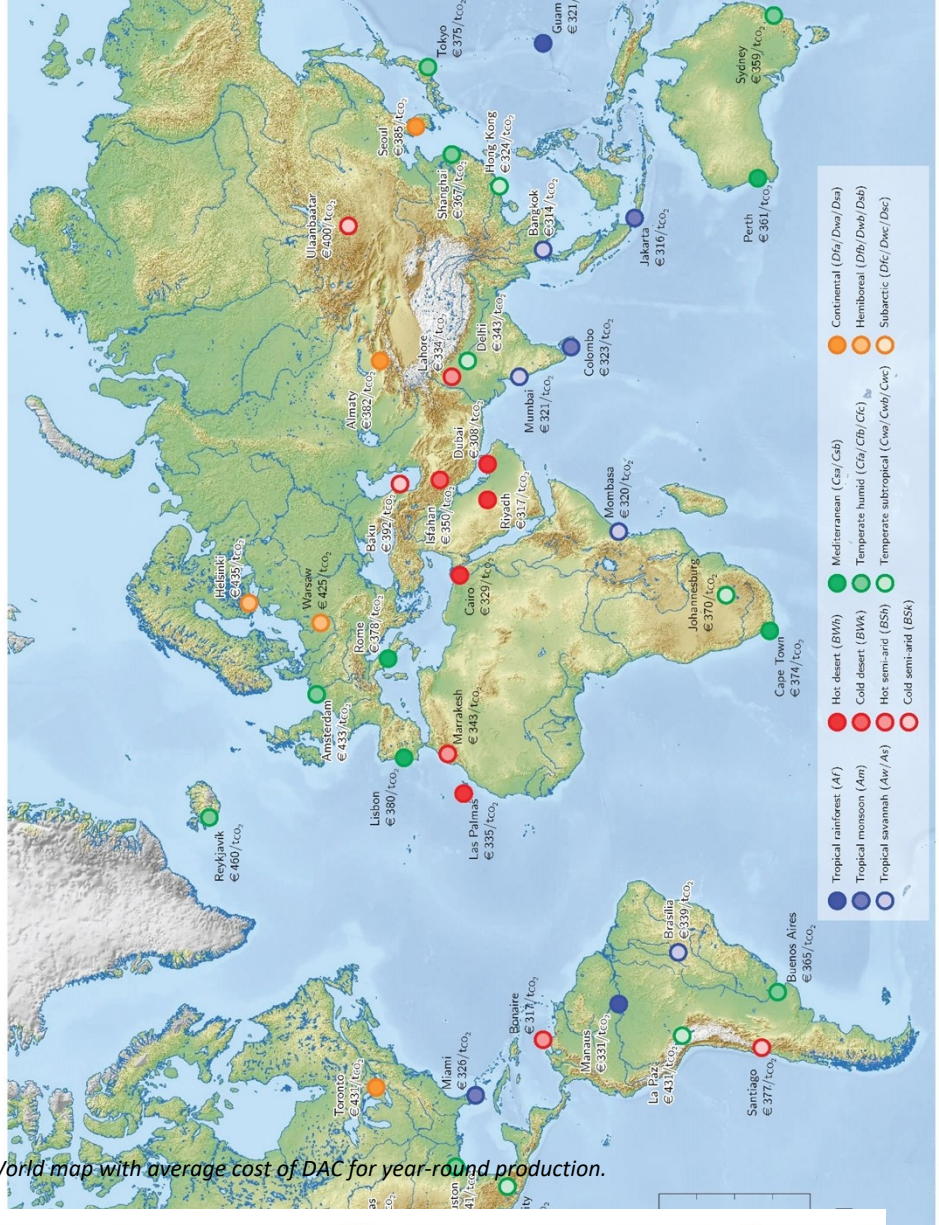

Figure 10 – World map with average cost of DAC for year-round production.

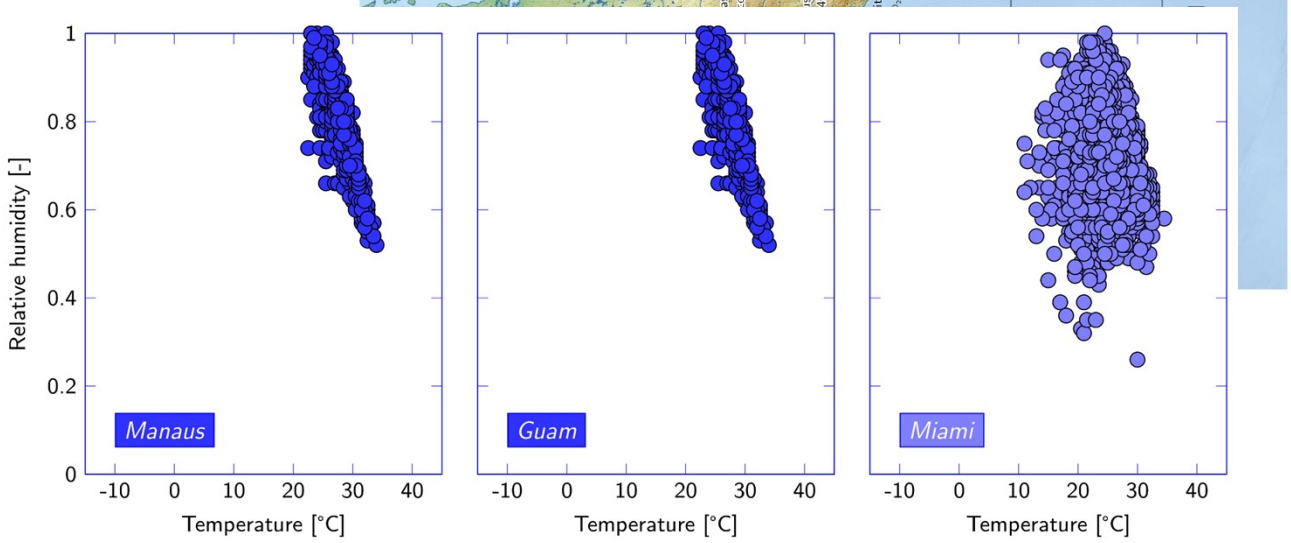

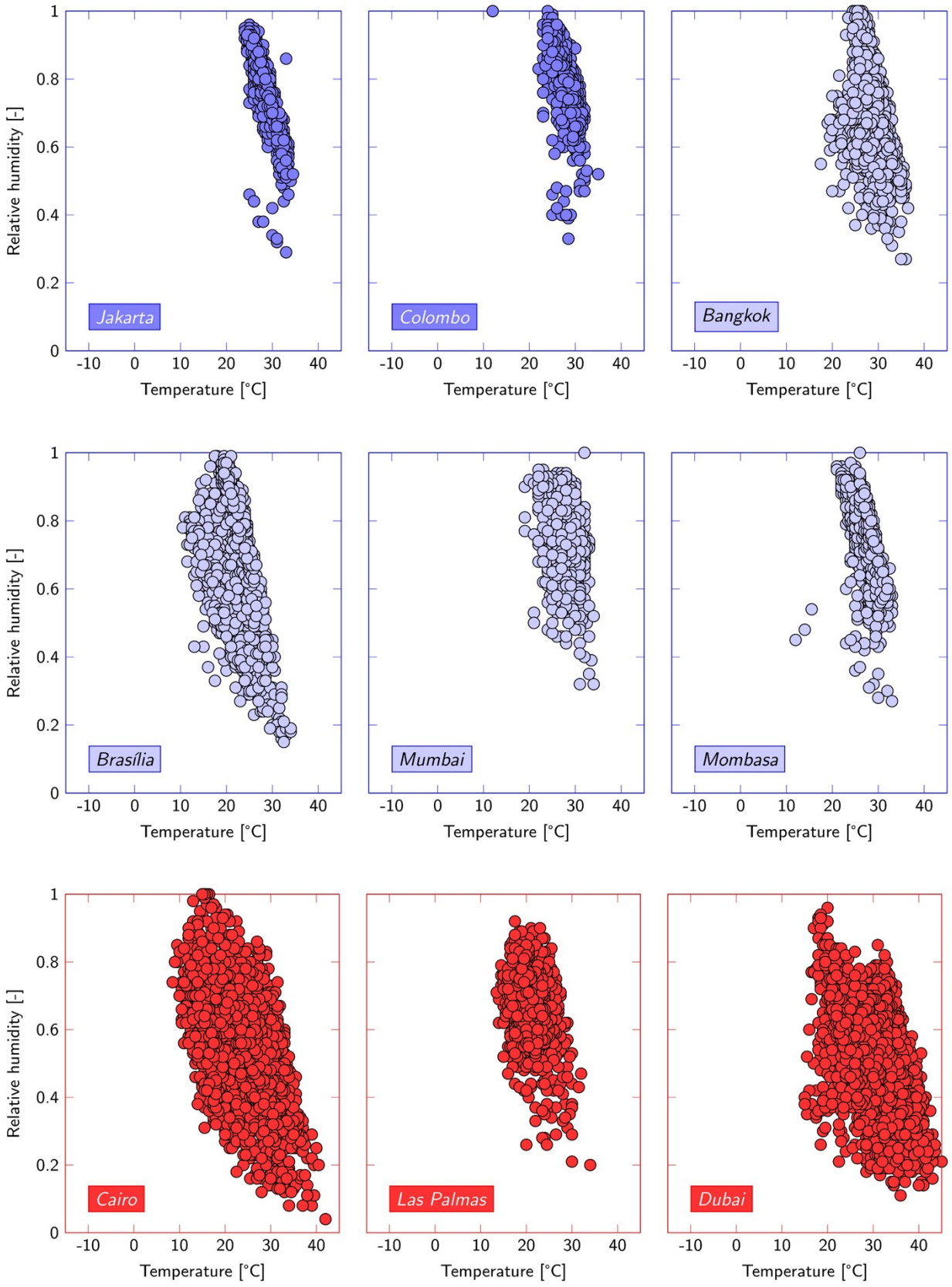
Relative humidity [-]
Temperature [°C]
Jakarta
Colombo
Bangkok
Brasília
Mumbai
Mombasa
Cairo
Las Palmas
Dubai

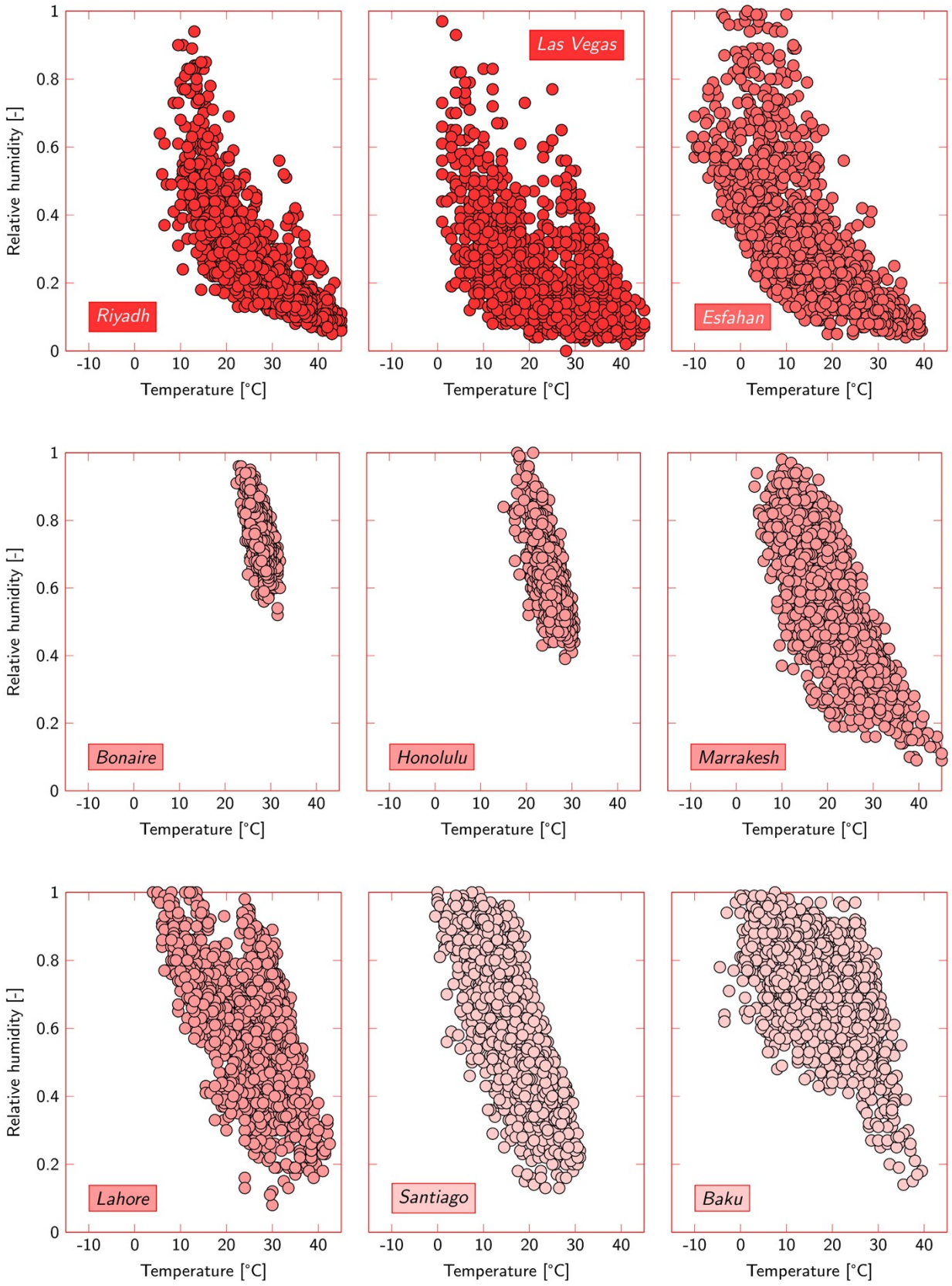
Riyadh
Las Vegas
Esfahan
Bonaire
Honolulu
Marrakesh
Lahore
Santiago
Baku
Relative humidity [-]
Temperature [°C]
0
0.2
0.4
0.6
0.8
1
-10
0
10
20
30
40

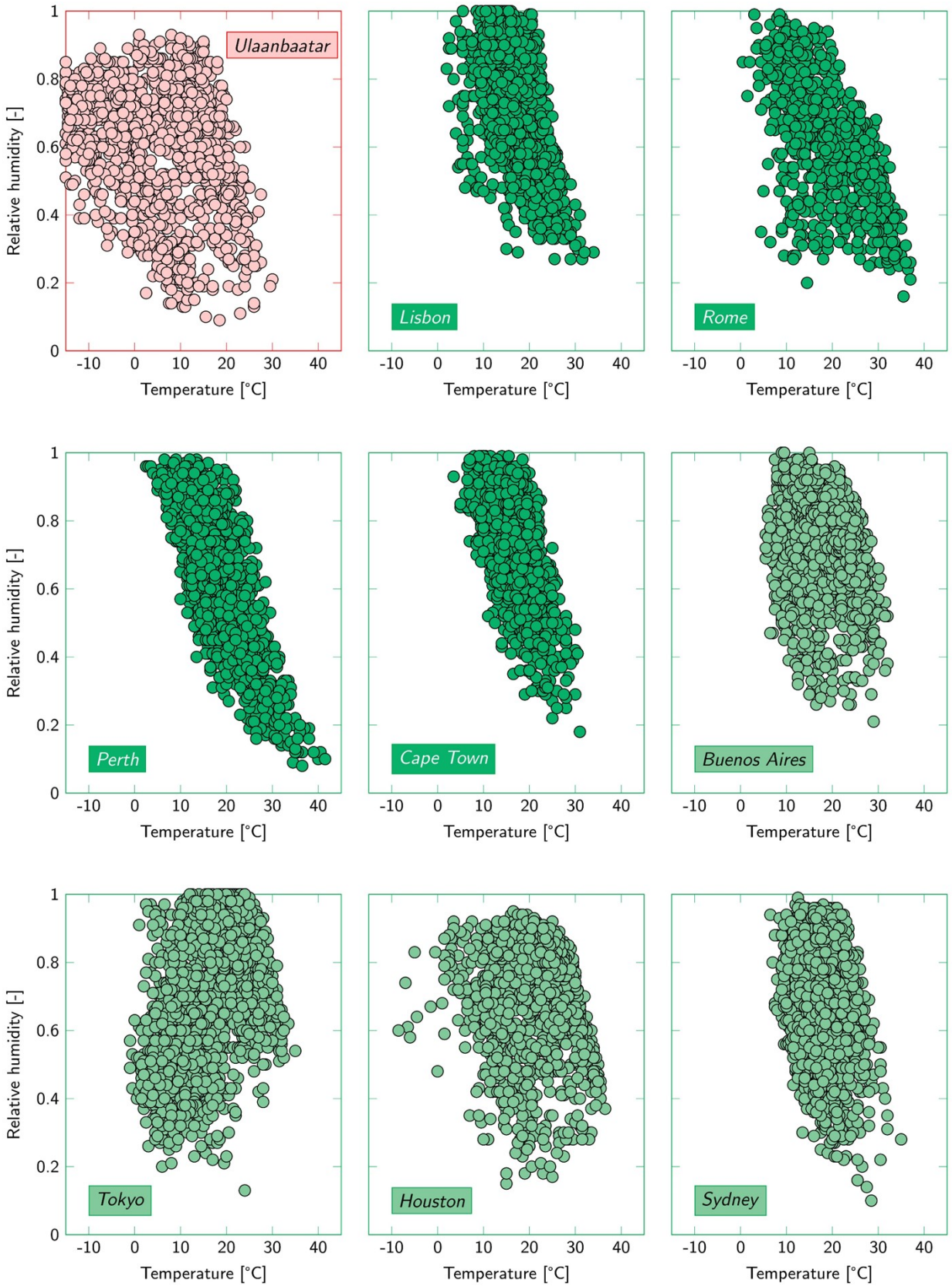
Ulaanbaatar
Lisbon
Rome
Perth
Cape Town
Buenos Aires
Tokyo
Houston
Sydney
Relative humidity [-]
Temperature [°C]
0
0.2
0.4
0.6
0.8
1
-10
0
10
20
30
40

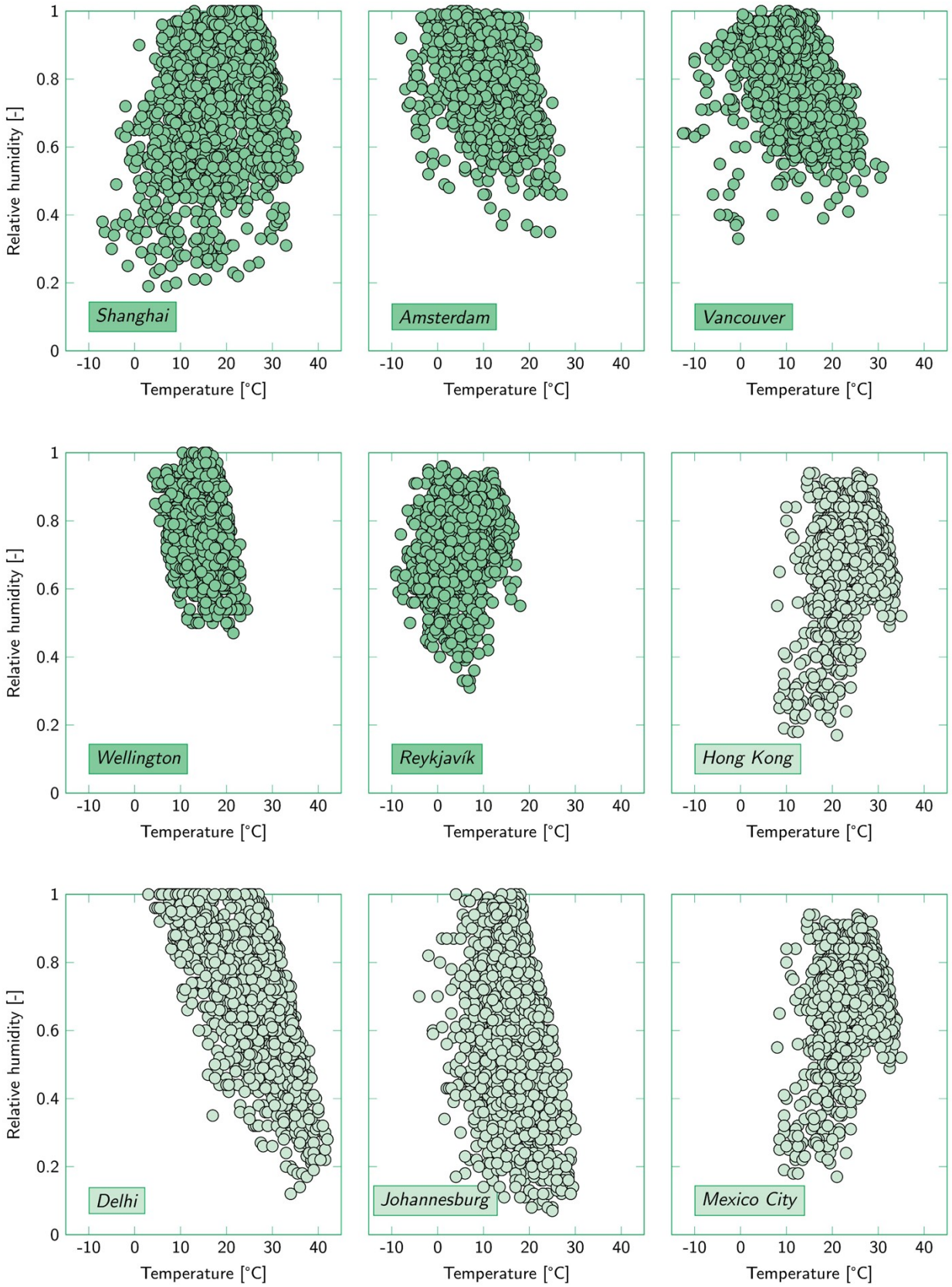
Relative humidity [-]
Temperature [°C]
Shanghai
Amsterdam
Vancouver
Wellington
Reykjavík
Hong Kong
Delhi
Johannesburg
Mexico City

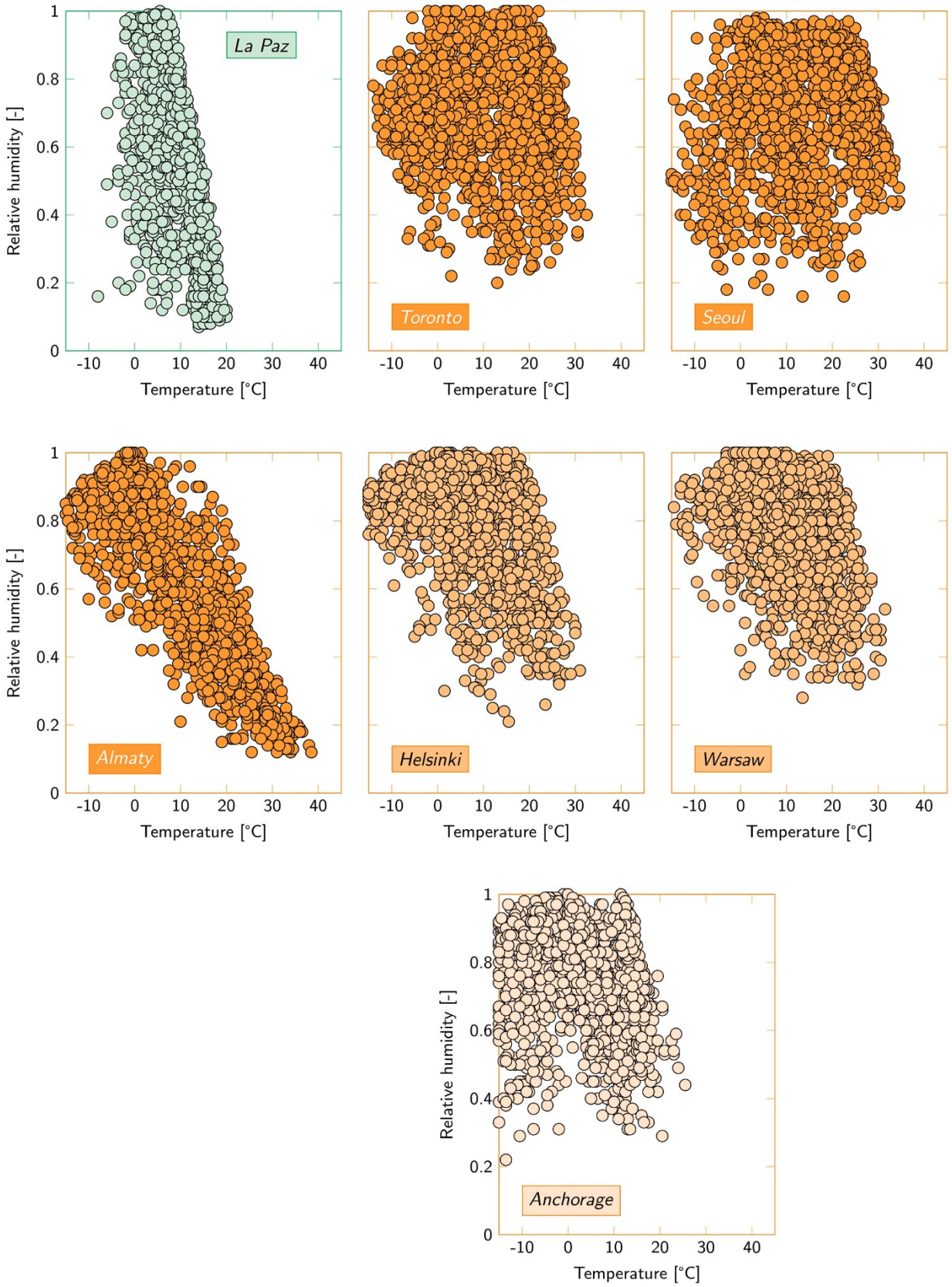

Figure 11 – Six-hour average weather data for 46 cities around the world with different climates. Data colours refer to the climate groups presented in Figure 10.[11]

6. Nomenclature

Symbol	Description	Unit
a	parameter for CO2 equilibrium capacity in humid conditions	-
b	Tóth affinity parameter	Pa^{-1}
b_0	Tóth affinity parameter at reference temperature	Pa^{-1}
C_p	specific heat capacity	$J\ kg^{-1}\ K^{-1}$
$C_{0,GAB}$	Arrhenius pre-exponential factor of C_{GAB}	-
C_{GAB}	Guggenheim constant in GAB isotherm	-
c	concentration	$mol\ m_g^{-3}$
D_{ax}	axial dispersion coefficient	$m_g^3\ m_r^{-1}\ s^{-1}$
D_p	effective pore diffusion coefficient	$m_g^3\ m_r^{-1}\ s^{-1}$
E_{act}	activation energy	$J\ mol^{-1}$
f_{enh}	enhancement factor	-
$\Delta_r H$	reaction enthalpy	$J\ mol^{-1}$
ΔH_C	difference in enthalpy between monolayer and multilayer	$J\ mol_{H2O}^{-1}$
ΔH_k	difference in enthalpy between bulk liquid and multilayer	$J\ mol_{H2O}^{-1}$
k_0	Arrhenius pre-exponential factor of reaction rate constant k_T or k_{LDF}	$mol_{CO2}\ kg_s^{-1}\ Pa^{-1}\ s^{-1}$ or s^{-1}
$k_{0,GAB}$	Arrhenius pre-exponential factor of k_{GAB}	-
k_{GAB}	multilayer correction factor in GAB isotherm	-
k_{LDF}	linear driving force reaction rate constant	s^{-1}
k_T	Tóth reaction rate constant	$mol_{CO2}\ kg_s^{-1}\ Pa^{-1}\ s^{-1}$
m	fit parameter for CO_2/H_2O co-adsorption correlation	$kg_s\ mol_{CO2}^{-1}$
n	fit parameter for CO_2/H_2O co-adsorption correlation	-
p	pressure	Pa
Q_{source}	energy source	$J\ m_r^{-3}\ s^{-1}$
q	sorbent loading	$mol\ kg_s^{-1}$
q_s	Tóth maximum sorbent loading	$mol_{CO2}\ kg_s^{-1}$
$q_{s,0}$	Tóth maximum sorbent loading at reference temperature	$mol_{CO2}\ kg_s^{-1}$
R	gas constant	$J\ mol^{-1}\ K^{-1}$
R_i	reaction rate of component i	$mol\ kg_s^{-1}\ s^{-1}$
r	radius	m
T	temperature	K
T_0	Tóth reference temperature	K
t	time	s
t_h	Tóth heterogeneity parameter	-
$t_{h,0}$	Tóth heterogeneity parameter at reference temperature	-
u_g	superficial gas velocity	$m_g^3\ m_r^{-2}\ s^{-1}$
V	volume	m^3
z	axial position	m

Greek symbols

α	temperature dependency parameter of t_h	-
ε	void fraction	-
η_i	effectiveness factor of component i	-
λ	thermal conductivity	$W\ m^{-1}\ K^{-1}$
ρ	density	$kg\ m^{-3}$
ϕ_{th}	Thiele modulus	-
χ	temperature dependency parameter of q_s	-

Subscripts

ads	adsorption
av	average
ax	axial direction
$bulk$	bulk phase
CO_2	carbon dioxide
eff	effective
eq	equilibrium
g	gas phase
H_2O	water
i	component
r	reactor
s	solid phase

Superscripts

dry	dry conditions
sat	saturation

7. References

1 R.T. Driessen, S.R.A. Kersten and D.W.F. Brilman, *Ind. Eng. Chem. Res.*, 2020, 59, 15, 6874–6885.

2 H.M. Schellevis, T.N. van Schagen and D.W.F. Brilman, *Int. J. Greenh. Gas Control.*, 2021, **110**, 103431.

3 H.M. Schellevis, PhD thesis, University of Twente, 2023.

4 M.J. Bos, T. Kreuger, S.R.A. Kersten and D.W.F. Brilman, Chem. Eng. J., 2019, 377, 120374.

5 H.M. Schellevis and D.W.F. Brilman, React. Chem. Eng., 2024, 10.1039/d3re00460k

6 M. Laumanns, L. Thiele and E. Zitzler, *European Journal of Operational Research*, 2006, **169**, 932.

7 M. Mesquita-Cunha, J.R. Figueira and A.P. Barbosa-Povoa, *European Journal of Operational Research*, 2023, **306**, 286.

8 C. Arpagaus, F. Bless, M. Uhlmann, J. Schiffmann and S.S. Bertsch, *Energy*, 2018, **152**, 985.

9 G. Towler and R. Sinnott, *Chemical Engineering Design*, Butterworth-Heinemann, Oxford, 2020.

10 IRENA, *Renewable Power Generation Costs in 2021*, International Renewable Energy Agency, Abu Dhabi, 2022.

11 World Temperatures - Weather Around The World, www.timeanddate.com/weather, (accessed: December 2023).